Controlled Pixelation of Inverse Opaline Structures Towards Reflection-Mode Displays

Su Yeon Lee, Shin-Hyun Kim, Hyerim Hwang, Jae Young Sim, and Seung-Man Yang*

Professor Yang passed away unexpectedly on September 26th 2013. We dedicate this work as a memorial to him.

A photonic bandgap in a material arises from periodic modulations in the refractive index of the material over a length scale that is half the wavelength of the light. Photons having an energy within the bandgap range cannot pass through the photonic crystals and are reflected.[1–3] Photonic crystals having a bandgap in the visible range exhibit sparking interference colors that are useful in colorimetric sensors, encoded microcarriers, and microdisplays.[4–8] Significant efforts have been applied toward preparing photonic crystals by crystallizing monodisperse colloidal particles. Regular arrays of colloids arranged in a crystalline structure spatially modulate the refractive index and, therefore, display opalescent structural colors.[9–12] One of most popular methods of preparing highly-ordered photonic colloidal crystals in a controllable manner involves convective assembly on a planar substrate.[13] In this approach, a substrate is dipped in a colloidal suspension and slowly pulled out. During the retraction step, the colloids concentrate near the meniscus on the substrate surface and form planar opal structures. The shape and properties of the colloidal crystals may be further controlled using a variety of techniques, including micromolding, inkjet printing, and photolithography.[14–24] These techniques enable the creation of microphotonic components or patterned photonic structures. For example, molding of colloids in microcapillaries or microchannels produces colloidal crystals with the shape of the mold.[14–16] Inkjet printing techniques have also enabled the deposition of droplet arrays composed of colloidal suspensions to produce photonic dome arrays.[17–19] Advanced micropatterns of photonic crystals have been prepared by photolithography. Colloids dispersed in photocurable resin are aligned or crystallized under an external field, and the resulting structures then are permanently fixed in polymerized resin by photolithography, making color patterns.[20,21] However, previous approaches have suffered from several intrinsic drawbacks that have severely limited their practical applications. Most opals templated by micromolds or droplets are fragile due to their low physical integrity. In addition, the minimum feature size of lithographically-featured micropatterns is too large or the reflectivity of the structures is insufficient for practical use. Photocurable resins used in the photolithographic techniques for patterning of colloidal crystals are monomers or prepolymers for radical polymerization rather than photoresist, thereby providing a limited feature resolution of micropattern. Furthermore, few methods can produce multicolored micropatterns with complex shapes. Therefore, there is a significant demand for practical and reproducible methods of preparing photonic crystal micropatterns with high controllability, definition, and reflectivity.

Here, we report a facile and straightforward method for preparing multi-colored inverse opal micropatterns by combining the convective assembly of colloidal particles with photolithographic techniques. Evaporation-induced convective assembly was used to vertically deposit colloidal crystals on the surface of a photoresist. The crystals were subsequently fully embedded in a photoresist matrix by capillary wetting during thermal annealing. Photolithography of the crystal embedded in the photoresist enabled the creation of composite micropatterned structures. Photoresist-based photolithography provided a high definition and flexibility on pattern shape. Selective removal of the colloids left behind regular cavities, forming an inverse opal structures with high index contrast between the air and the polymerized photoresist. The structure provides high reflectivity at the wavelength of bandgap. In addition, the monolithic crosslinked inverse opals displayed high mechanical stability. The crystal deposition and photolithography procedure is repeatable and provides a general means for preparing multi-colored micropatterns of inverse opals. With this flexible approach, we pixelated inverse opals with three distinctive squares of red (R), green (G), and blue (B) structural colors, each of which has different cavity size. This kind of pixelated color pattern is a prerequisite for implementation of color display device operated at reflection mode.

The procedure for preparing single-colored micropattern of inverse opals is illustrated in **Figure 1**a. Highly-ordered colloidal crystals were prepared on the photoresist surface using the vertical deposition method.[13] A negative photoresist, SU-8, was spin-coated onto a silicon wafer with a thickness, t_{PR}, of 10 μm and treated with oxygen plasma to render the surface hydrophilic. The substrate was dipped in an aqueous suspension of monodisperse silica particles of diameter 278 nm and slowly pulled out of the solution. The silica particles formed a face-centered cubic (fcc) structure, that is, an opal structure, on the surface of the SU-8, as shown in the cross-sectional scanning electron microscopy (SEM) image of Figure 1b. Because the fcc crystals grow from the surface of SU-8, the (111) plane of the fcc lattice is always aligned along the surface. The thickness of the opal film, t_O, depended on the pulling speed and

Dr. S. Y. Lee, Prof. S.-H. Kim, H. Hwang, J. Y. Sim, Prof. S.-M Yang
Department of Chemical and Biomolecular Engineering, KAIST
Daejeon, 305–701, Korea
E-mail: kim.sh@kaist.ac.kr
Dr. S. Y. Lee, H. Hwang, J. Y. Sim, Prof. S.-M. Yang
National Creative Research Initiative Center for Integrated Optofluidic Systems KAIST
Daejeon 305–701, Korea

DOI: 10.1002/adma.201304654

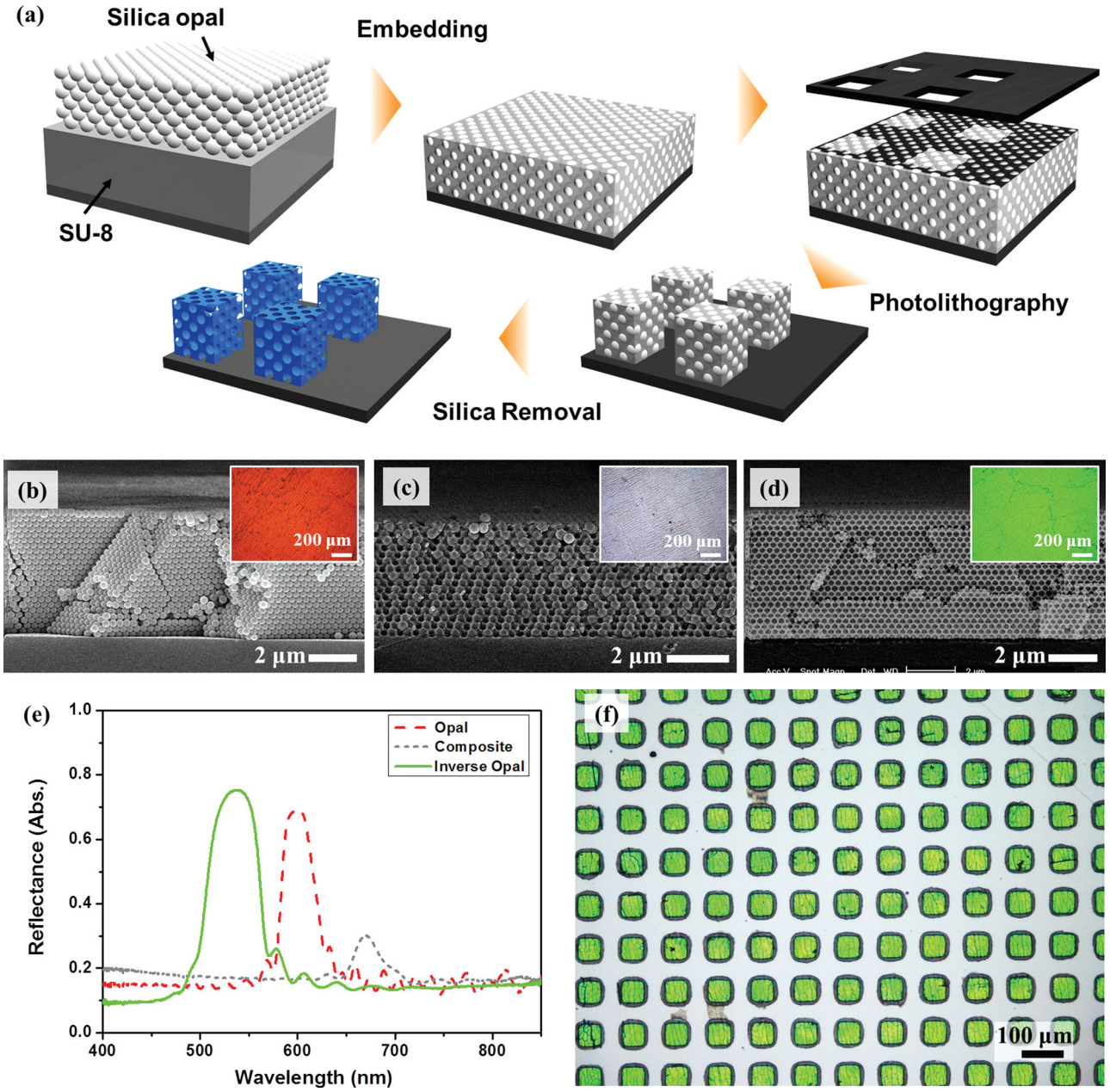

Figure 1. (a) Schematic diagram illustrating the formation of a pixelated inverse opal by embedding an opal film in a negative photoresist (SU-8), applying photolithography, and removing the silica particles. (b–d) Cross-sectional scanning electron microscopy (SEM) images of the opal, composite, and inverse opal films. The insets in each panel show the optical microscopy (OM) images of the films. (e) The reflectance spectra of the films shown in (b–d); opal and composite indicate the spectra from the opal on the surface of SU-8 before embedding and the opal embedded in the SU-8, respectively. (f) OM image of a pixelated inverse opal prepared to reflect green light.

the concentration of silica particles. We prepare a 6 μm thick opal film, as shown in Figure 1b. The silica opal film displayed a uniform red color from the reflection at the top surface of the stacked multilayered (111) planes, as shown in the inset of Figure 1b. The bandgap position, λ, could be estimated from Bragg's law applied to the (111) plane of the fcc structure:[4]

$$\lambda = 2dn_{eff} = \left(\frac{8}{3}\right)^{1/2} Dn_{eff} \quad (1)$$

where d is the (111) plane spacing, n_{eff} is the effective refractive index, D is the particle diameter. To determine n_{eff}, we use

$$n_{eff} = \left(\phi_p n_p^2 + (1-\phi_p) n_m^2\right)^{1/2} \quad (2)$$

where ϕ_p is the volume fraction of particles, and n_p and n_m are the refractive indices of the particle and matrix, respectively. For fcc colloidal crystal (ϕ_p = 0.74) composed of silica particles (n_p = 1.42) with D = 278 nm, Bragg's law predicted

a λ = 601 nm, in good accord with the reflectance spectrum obtained from the opal film, as denoted by the red dotted line in Figure 1e; periodic peaks in the spectra are Fabry-Perot fringes which are generated by thin film interference. The normalized full width at half maximum (FWHM) which is the ratio of the FWHM to the peak position wavelength, $\Delta\lambda/\lambda$, was roughly proportional to the normalized index contrast, $\Delta n/n_{eff}$, where Δn is $|n_p - n_m|$.[25] The value of $\Delta\lambda/\lambda$ was 0.0603 for an opal having $\Delta n/n_{eff}$ of 0.3173.

The silica opal became embedded in the photoresist upon thermal annealing at a temperature of 120 °C, which exceeded the glass transition temperature (T_g) of the uncrosslinked SU-8, 55 °C. The spontaneous embedding process was driven by capillary wetting of the molten SU-8 onto the surfaces of the silica opals; the embedding of silica particles replaces the high energy interface of silica-air with the low energy interface of silica-SU-8. During the embedding process, the fcc structure remained undisturbed and the interstices between particles became filled with SU-8; van der Waals attraction between silica particles holds the fcc structure during infiltration of SU-8 through interstices. For sufficiently thick SU-8 film, the embedding is completed when top layer of opal film, (111) plane of fcc lattice, is anchored at the interface between air and molten SU-8, being partially exposed to air, as shown in Figure 1c. The top surface displayed a hexagonal array of small bumps and particle-free SU-8 layer remains below the composite layer.[26,27] For $t_{PR} > (1-\varphi_p)t_O$, the opal was fully embedded except for the top layer, resulting in a total thickness, t_T, determined by the sum of the thickness of the composite layer, t_C, and the thickness of the particle-free residual layer, t_R:

$$t_T = t_c + t_R = t_o + \left(t_{PR} - \left(1-\varphi_p\right)t_o\right) = t_{PR} + \varphi_p t_o \quad (3)$$

The composite film had a thickness of 14.5 μm, as expected based on Equation (3). The film exhibits negligible reflection colors and low reflectivity, as shown in the inset of Figure 1c and the gray dotted line in Figure 1e, respectively; these are attributed to small index contrast between silica particles (n_p = 1.42) and SU-8 (n_m = 1.6). The reflectance peak was red-shifted to 667 nm from that of the opal, in good agreement with Equation (1).

The index contrast was significantly enhanced by selectively removing the silica particles. The silica particles were etched away by treating the sample with a dilute hydrofluoric acid (HF) solution that left behind an array of air cavities, as shown in Figure 1d. This inverse opal structure had a high index contrast, Δn, of 0.6, resulting in a vivid reflected color and a high reflectivity, as shown in the inset of Figure 1d and denoted by the green solid line in Figure 1e, respectively; reflectivity is as high as 80%. The normalized FWHM, $\Delta\lambda/\lambda$, also increased to 0.1033 as the value of $\Delta n/n_{eff}$ increased to 0.5061. The bandgap position was blue-shifted to 538 nm due to a decrease in the effective refractive index, consistent with Equation (1).

The inverse opal could be patterned using photolithography. After embedding the colloidal crystals into the SU-8 photoresist, a photomask was used to selectively illuminate the sample with UV light. The photomask included transparent squares with dimensions of 50 μm × 50 μm that formed square arrays with a periodicity of 100 μm. The SU-8 in the UV-irradiated regions became crosslinked after applying a post-exposure baking step and remained on the substrate after developing the uncrosslinked SU-8. The subsequent removal of silica particles yielded an inverse opal micropattern, as shown in Figure 1f, where each square exhibited a bright green color. An SEM image of the micropattern is shown in Figure S1a of the Supporting Information, which reveals a layer thickness of 14.5 μm, in agreement with Equation (3). The boundary of the squares appears slightly blunt. We attribute this to scattering of UV light by silica particles embedded in SU-8 film during UV exposure.

The bandgap position (reflection color) of the inverse opal was determined by the size of the air cavities. The color could, therefore, be controlled by adjusting the particle size, as described by Equation (1). For example, inverse opal micropatterns having three distinctive R, G, and B colors could be prepared by using three different silica particle sizes, as shown in **Figure 2**a–2c. Silica particles with diameters of 343 nm, 278 nm, and 249 nm were used to implement the structural colors R, G, and B, respectively. An optical microscopy image of the blue squares, taken at a low magnification, is shown in Figure S1b. The top surface of the inverse opals displayed a hexagonal array of circular holes, as shown in the insets of Figure 2a–2c. The surface features provided additional evidence that the top layer of the opal was anchored at the interface between air and molten SU-8 during annealing. The hole size and inter-hole distance were determined by size of templating silica particles. Larger particles produced larger lattice constants and, therefore, longer wavelength of bandgap position. The reflectance spectra of the inverse opal films prepared from the same silica particles are shown in Figure 2d; peaks are located at 665 nm (R), 538 nm (G), and 482 nm (B), consistent with the values predicted using Equation (1). All three spectra had reflectivities as high as 70–80%, and the values of $\Delta\lambda/\lambda$ were 0.1047, 0.1033, and 0.1068, which were self-consistent.

Multi-colored inverse opal patterns could be prepared by performing multiple sets of crystal deposition and photolithography, as illustrated schematically in **Figure 3**a. After the silica/SU-8 composite micropattern had been prepared by following the procedure described previously (steps 1–4 in Figure 1a), the SU-8 photoresist was spin-coated over the pattern. The interstices between the squares were then filled with SU-8. An ultra-thin film formed on the top surface of the squares, as shown in Figures S2a and S2b of the Supporting Information. We deposited colloidal crystals onto the surface of this planar SU-8 film after oxygen plasma treatment. Silica particles of different sizes were used to create distinct colors. Subsequent thermal annealing at 120 °C selectively embedded the colloidal crystals only at the interstitial sites created by the preformed squares; the crosslinked SU-8 in the squares did not melt, thereby retaining opal structure on the top of composite squares. During the embedding process, the total SU-8 film thickness in the interstices increased, whereas the total thickness of the SU-8 film in the crosslinked squares remained constant. This makes the thicknesses of the two types of squares slightly different; the difference is $\phi_p t_O$. This also makes gap between photomask and silica-embedded SU-8 film during second step of photolithography; this gap distance is $(1-\phi_p)t_O$. For typical opal film with 5 μm in thickness, the gap is 1.3 μm, which is acceptable for

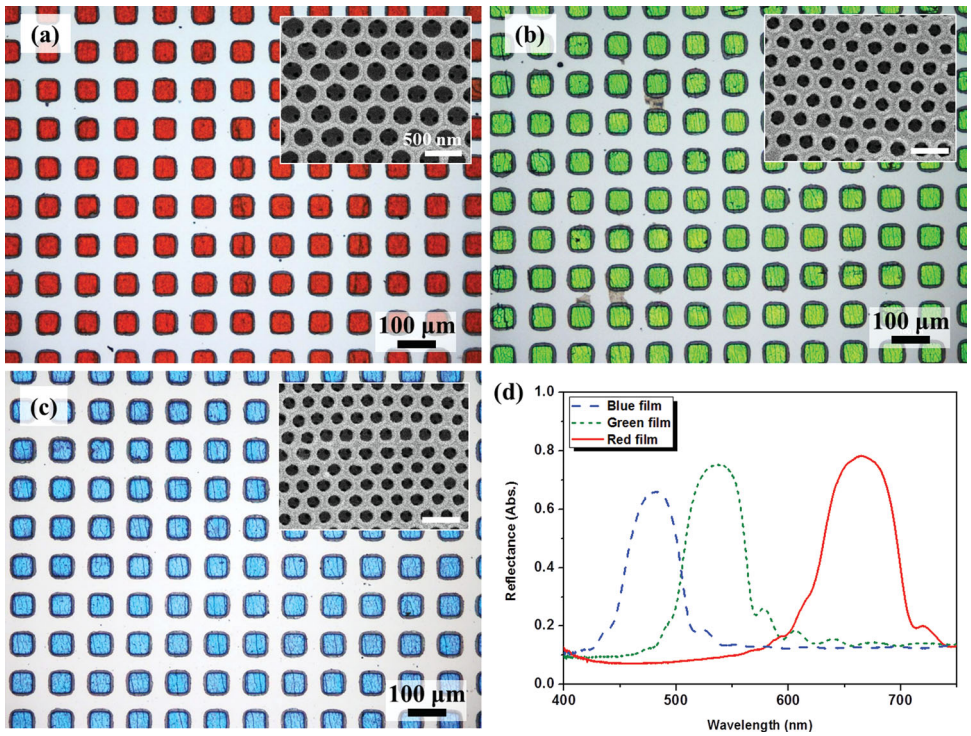

Figure 2. (a–c) OM images of the pixelated inverse opals prepared to reflect a single color. The inverse opals were templated from the opals composed of silica particles of diameter (a) 343, (b) 278, or (c) 249 nm. The insets in each panel show the hexagonal arrays of air cavities on the top surfaces of the pixels. (d) The reflectance spectra of the inverse opal films that had been templated by the opals used to prepare (a–c).

high definition pattering. The aligned photomask containing an array of transparent squares permitted the selective illumination of UV light onto the interstices. The uncrosslinked SU-8 was developed after applying a post-exposure baking step, yielding a micropattern having two distinct squares of composite structures: one formed by the first photolithography step and the other formed by the second. Removal of the silica particles yielded a dual-colored inverse opal micropattern. Three combinations of two different colors among R, G, and B were prepared. Figures 3b–3d show photographs of these micropatterns: R plus G, G plus B, and B plus R, where the R, G, and B pixels were created by silica particles with diameters of 343, 278, and 249 nm, respectively. An optical microscopy image of the pattern prepared with R plus G was taken at a lower magnification and is shown in Figure S2c. These patterns show an aligned alternating pattern of two types of squares reflecting different colored light and having different heights. The pattern formed rows with a regular spacing. The height of the preformed squares was lower than the height of the post-formed squares, as shown in Figure S2d of the Supporting Information. The height difference was $\phi_p t_O$ for the case in which the SU-8 film applied to the interstices had the same thickness as the thickness of the preformed squares. In reality, the SU-8 film was slightly concave, as shown in Figure S2a, thereby reducing the height difference to be approximately 4 μm. The reflectance spectra of the dual-colored patterns are shown in Figure 3e. Each spectrum displayed two distinct peaks formed by the superposition of the two reflection spectra. The reflectivity was significant, considering that each pixel occupied only 25% of the total area.

The same procedure was used to prepare other dual-colored pattern designs. For example, an array of R squares in a G matrix could be obtained, as shown in **Figures 4**a and 4b. This pattern was prepared using a photomask containing transparent squares for the creation of R squares, followed by a second photomask with the inverted pattern, non-transparent squares, for the creation of the G matrix. The height of the R squares was lower than that of the matrix, as shown in the SEM image of Figure 4c. Moiré fringes appeared due to the interaction between the regular lattice of air cavities and the SEM scanning line pattern. The Moiré fringes provided evidence in support of a high degree of structural regularity.[28] The regular array of air cavities can be observed at high magnification levels, as shown in Figure 4d. Because the embedding process did not interfere with the opal structure, the resultant inverse opals had an array of air cavities that was interconnected through small windows. Any combination of the two colors could be introduced into the pattern. For example, G squares in an R matrix and B squares in an R matrix could be prepared, as shown in Figures S3a and S3b of the Supporting Information, respectively. In addition, size of the squares can be reduced to achieve high definition. For example, dual-colored arrays composed of 15 μm blue squares and 50 μm red squares could be prepared as shown in Figure S4 of the Supporting Information.

During the second crystal deposition and photolithography steps, the inverse opals maintained their structures with no deterioration in optical properties. Additional steps could, therefore, be applied to enrich the variety of structural colors. For example, additional pixels could be created on the

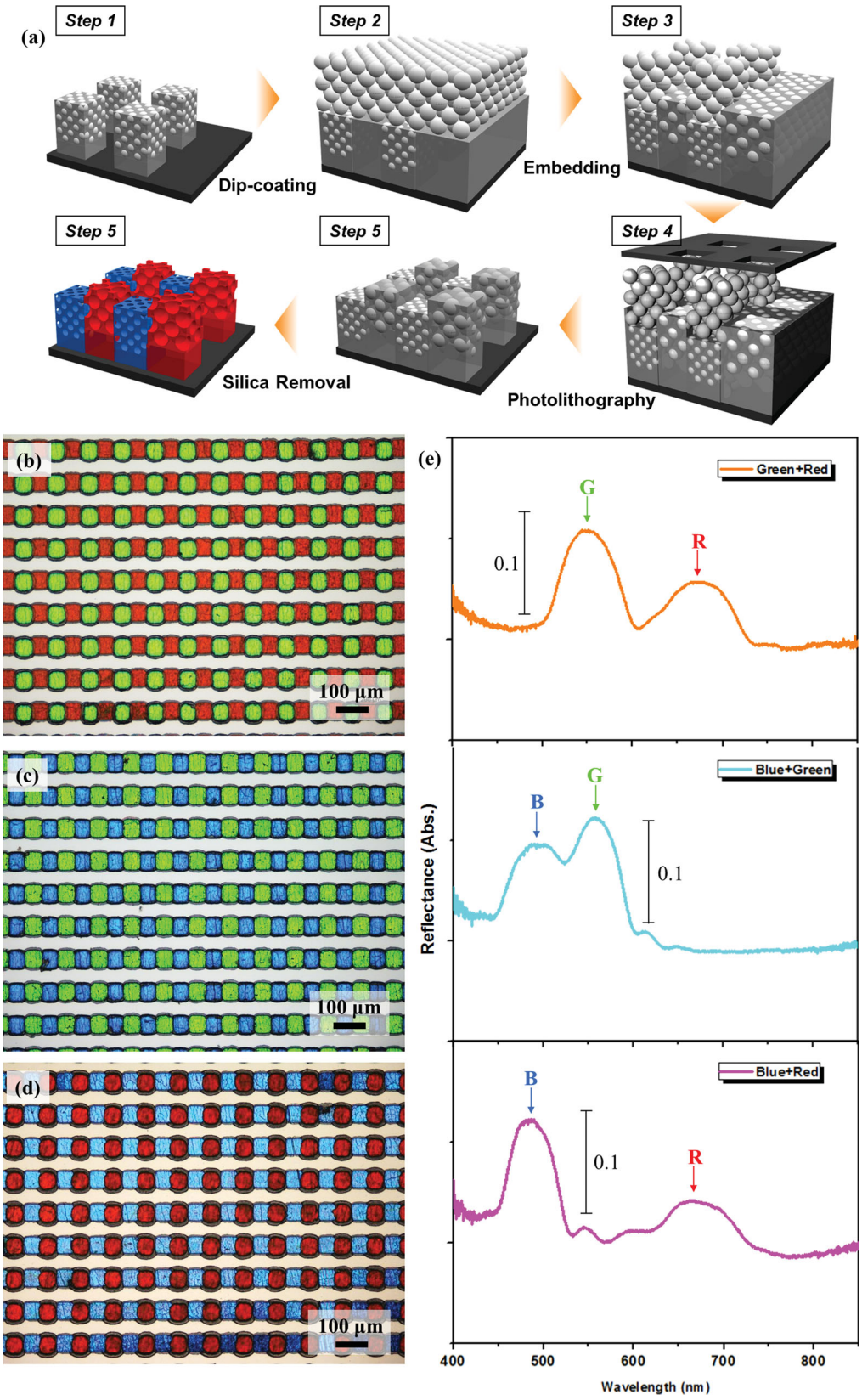

Figure 3. (a) Schematic diagram illustrating the preparation of a pixelated inverse opal prepared to reflect two distinct colors. (b–d) OM images of dual-color pixelated inverse opals: (b) red and green, (c) green and blue, and (d) blue and red. (e) Reflectance spectra of the pixelated inverse opals shown in (b–d), where each spectrum displayed two distinct peaks, as indicated by the arrows.

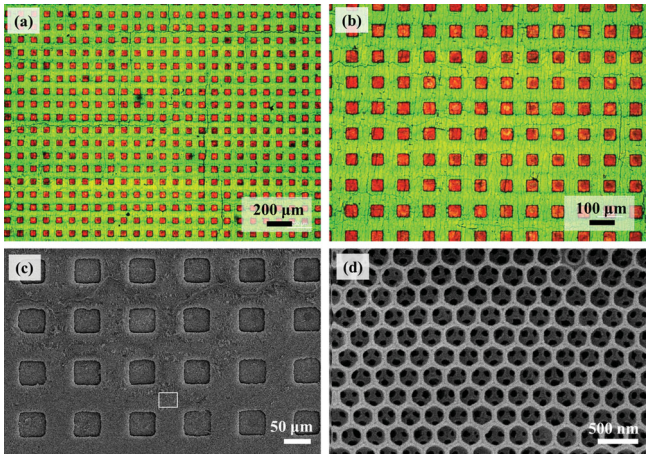

Figure 4. (a, b) OM images of the pixelated inverse opal composed of an array of red squares in a green matrix. (c) SEM image of the pixelated inverse opal. (d) Magnified view of the green matrix with a hexagonal array of air cavities.

dual-colored pattern shown in Figure 3. The fabrication procedures described above were applied three times to create R, G, and B reflector pixels in a single pattern, as shown in **Figures 5**a and 5b. The three inverse opal squares and one empty square formed one unit of the pixels, as denoted in the box in Figure 5b. The three squares had different heights, as shown in Figure 5c. The bottom right corner in each unit was empty, the top left corner had the lowest height of 14.5 μm (created using the first step), the top right corner had the intermediate height of 18.9 μm (created using the second step), and the bottom left corner had the greatest height of 23.3 μm (created using the third step), where the heights were estimated by Equation (3). The reflectance spectrum from this pixelated inverse opal films exhibited three peaks centered at wavelengths of 665 nm, 538 nm, and 482 nm, as indicated by the arrows in Figure 5d. Each peak was contributed by a distinct square. Pixelated color reflectors are required for the fabrication of color display devices operated in the reflection mode.

A similar approach was taken to create porous structures in which the air cavities were randomly packed. These structures were white rather than sparkling because Mie scattering by the disordered medium is wavelength-independent.[29,30] These structures were prepared by forming a colloidal glass having disordered structures of particles on a pre-coated SU-8 layer using the vertical deposition method. An aqueous mixture containing 2 wt% silica particles with a diameter of 260 nm and 0.05 M $CaCl_2$ was used to prepare the colloidal glass. The positive calcium ions screened out the negative charges on the silica particles and destabilized the suspension by significantly reducing the electrostatic repulsion between silica particles. This induced the formation of random silica particle aggregates during the vertical deposition process, as shown in Figure S5a of the Supporting Information. This colloidal glass could be embedded into an SU-8 film, as shown in Figure S5b, and transformed into a porous glass by removing the silica particles, as shown in Figure S5c. The porous glass structure could be inserted into the empty spots of a pixelated pattern of the R, G, and B squares in Figure 5 to add white (W) pixels. White pixels can increase the brightness of a display device. Using an additional step involving glass deposition and photolithography, four distinct R, G, B, and W pixels were created, as shown in Figure S5d. The four squares formed a single unit of pixels as denoted in the box.

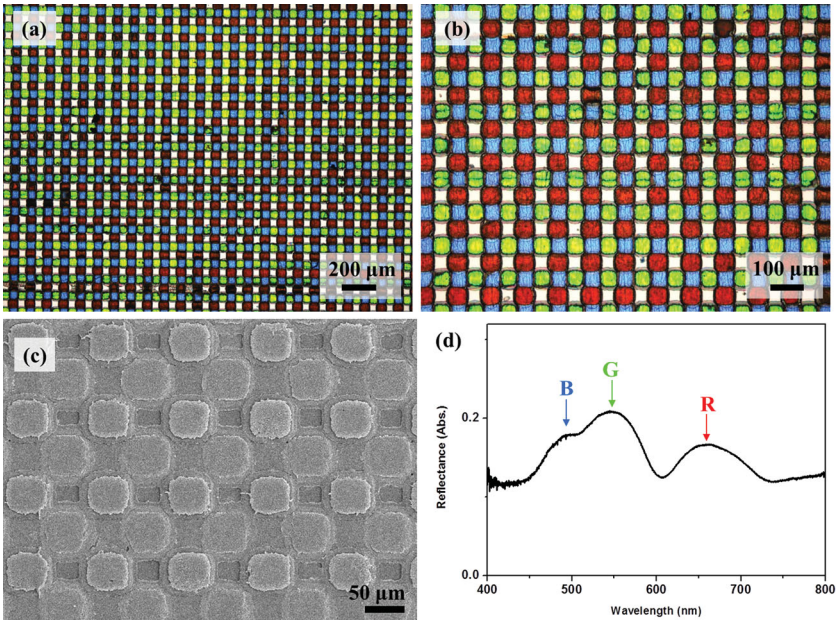

Figure 5. (a, b) OM images of the pixelated inverse opal prepared to have three distinct squares reflecting red, green, or blue colors. (c) SEM image of the pixelated inverse opal. A white rectangle denotes a single pixel unit. (d) Reflectance spectrum of the pixelated inverse opal, showing the presence of three distinct peaks, as indicated by the arrows.

In this work, we describe the development of a practical method for creating multicolored inverse opal micropatterns by hybridizing convective self-assembly of colloidal particles with photolithographic techniques. Colloidal crystals, prepared by vertical deposition, were embedded into a photoresist, and the composite was patterned using conventional photolithography. Subsequent removal of the colloids from the polymerized photoresist increased the refractive index contrast, yielding an inverse opal micropattern with vivid reflected colors. Multiple crystal deposition and photolithography steps enabled the creation of multi-colored patterns with a high degree of control over the pattern shape, size, and color. Moreover, this method provides high definition of micropattern and high reflectivity at the bandgap position. These advantages were combined to demonstrate the preparation of a square array of R, G, and B pixels, which are potentially useful for color display devices operated in the reflection mode. Therefore, our general approach to creating 3D photonic crystal micropatterns provides a new approach to the development of a wide range of photonic applications.

Experimental Section

Deposition of the colloidal crystals and subsequent embedding into the SU-8 photoresist: The negative photoresist SU-8, (Microchem) was spin-coated onto a silicon wafer to a thickness of 10 μm. Soft-baking at 95 °C for 5 min was used to evaporate the solvent. Prior to depositing the colloidal particles, the SU-8 film was treated with oxygen plasma for 60 s to render the surface hydrophilic. The substrate was vertically dipped into a 2 wt% aqueous suspension of monodisperse silica particles and was slowly pulled out at a speed of 0.25–0.80 μm/s to deposit the colloidal crystals in a controlled thickness. Three different silica particle sizes were used: 249, 278, or 343 nm (in diameter). The colloidal crystal composed of silica particles was then embedded into the SU-8 film during thermal annealing at 120 °C for 5 min on a hot plate.

Patterning of the inverse opal films: The colloidal crystal-embedded SU-8 film was exposed to UV light with a wavelength of 365 nm and intensity of 14.5 mW/cm^2 from an Hg lamp through a photomask for 15 s; this results in total UV dose of 217.5 mJ/cm^2. The film was post-exposure baked at 55 °C for 20 min. The unexposed photoresist was developed using propylene glycol methyl ether acetate (PGMEA, Sigma-Aldrich) and then rinsed with isopropyl alcohol. To remove the silica particles from the composite film, the composite pattern was immersed in a 5% HF solution (50%, Sigma-Aldrich) for 5 min; this is enough time to dissolve all silica particles in the composite film into the solution. The film was washed with distilled water several times and then subjected to complete drying.

Characterization: The structures of the opals, silica/SU-8 composites, and inverse opals were imaged using optical microscopy in the reflection mode (Nikon, L150), and SEM (Philips, XL30SFEG). The reflectance spectra were obtained using a spectrometer (OceanOptics Inc., USB4000) mounted on the optical microscope, where 10× lens was used; measurement spot has approximately 1.5 mm in diameter. For a light source, typical halogen lamp mounted on the microscope was used and all spectra from samples were normalized with spectrum of the light source which was measured with total mirror.

Supporting Information

Supporting Information is available from the Wiley Online Library or from the author.

Acknowledgements

This work was supported by a grant from the Creative Research Initiative Program of the Ministry of Education, Science and Technology for "Complementary Hybridization of Optical and Fluidic Devices for Integrated Optofluidic Systems." This work was supported by a National Research Foundation of Korea (NRF) grant funded by the Korean Government (MSIP) (Project No. 2006-0050630) and KAIST VRPGP (Project No. N01130054).

Received: September 17, 2013
Revised: November 12, 2013
Published online: January 23, 2014

[1] T. A. Taton, D. J. Norris, *Nature* **2002**, *416*, 685.
[2] Y. Xia, B. Gates, Y. Yin, Y. Lu, *Adv. Mater.* **2000**, *12*, 693.
[3] C. Lopez, *Adv. Mater.* **2003**, *15*, 1679.
[4] J. H. Holtz, S. A. Asher, *Nature* **1997**, *389*, 829.
[5] Y. J. Zhao, X. W. Zhao, J. Hu, M. Xu, W. J. Zhao, L. G. Sun, C. Zhu, H. Xu, Z. Z. Gu, *Adv. Mater.* **2009**, *21*, 569.
[6] S. H. Kim, S. J. Jeon, W. C. Jeong, H. S. Park, S. M. Yang, *Adv. Mater.* **2008**, *20*, 4129.
[7] A. C. Arsenault, D. P. Puzzo, I. Manners, G. A. Ozin, *Nat. Photonics* **2007**, *1*, 468.
[8] T. S. Shim, S. H. Kim, J. Y. Sim, J. M. Lim, S. M. Yang, *Adv. Mater.* **2010**, *22*, 4494.
[9] S.-H. Kim, S. Y. Lee, S.-M. Yang, G.-R. Yi, *NPG Asia Mater.* **2011**, *3*, 25.
[10] E. Yablonovitch, *Phys. Rev. Lett.* **1987**, *58*, 2059.
[11] I. I. Tarhan, G. H. Watson, *Phys. Rev. Lett.* **1996**, *76*, 315.
[12] Y. Xia, B. Gates, Z.-Y. Li, *Adv. Mater.* **2001**, *13*, 409.
[13] P. Jiang, J. F. Bertone, K. S. Hwang, V. L. Colvin, *Chem. Mater.* **1999**, *11*, 2132.
[14] E. Kim, Y. N. Xia, G. M. Whitesides, *Adv. Mater.* **1996**, *8*, 245.
[15] G. A. Ozin, S. M. Yang, *Adv. Funct. Mater.* **2001**, *11*, 95.
[16] S. M. Yang, H. Miguez, G. A. Ozin, *Adv. Funct. Mater.* **2002**, *12*, 425.
[17] K. Burkert, T. Neumann, J. J. Wang, U. Jonas, W. Knoll, H. Ottleben, *Langmuir* **2007**, *23*, 3478.
[18] J. Park, J. Moon, H. Shin, D. Wang, M. Park, *J. Colloid Interface Sci.* **2006**, *298*, 713.
[19] S. H. Kim, J. M. Lim, W. C. Jeong, D. G. Choi, S. M. Yang, *Adv. Mater.* **2008**, *20*, 3211.
[20] H. Kim, J. P. Ge, J. Kim, S. Choi, H. Lee, H. Lee, W. Park, Y. Yin, S. Kwon, *Nat. Photonics* **2009**, *3*, 534.
[21] H. S. Lee, T. S. Shim, H. Hwang, S. M. Yang, S. H. Kim, *Chem. Mater.* **2013**, *25*, 2684.
[22] C. E. Finlayson, P. Spahn, D. R. E. Snoswell, G. Yates, A. Kontogeorgos, A. I. Haines, G. P. Hellmann, J. J. Baumberg, *Adv. Mater.* **2011**, *23*, 1540.
[23] H. B. Hu, J. Tang, H. Zhong, Z. Xi, C. L. Chen, Q. W. Chen, *Sci. Rep.* **2013**, *3*, 1484.
[24] L. Mishchenko, B. Hatton, M. Kolle, J. Aizenberg, *Small* **2012**, *8*, 1904.
[25] M. N. Shkunov, Z. V. Vardeny, M. C. DeLong, R. C. Polson, A. A. Zakhidov, R. H. Baughman, *Adv. Funct. Mater.* **2002**, *12*, 21.
[26] S. Y. Lee, S. H. Kim, C. J. Heo, H. Hwang, S. M. Yang, *Phys. Chem. Chem. Phys.* **2010**, *12*, 11861.
[27] S. Y. Lee, S. H. Kim, S. G. Jang, C. J. Heo, J. W. Shim, S. M. Yang, *Anal. Chem.* **2011**, *83*, 9174.
[28] G. Subramania, K. Constant, R. Biswas, M. M. Sigalas, K. M. Ho, *Adv. Mater.* **2001**, *13*, 443.
[29] P. Wochner, C. Gutt, T. Autenrieth, T. Demmer, V. Bugaev, A. D. Ortiz, A. Duri, F. Zontone, G. Grubel, H. Dosch, *Proc. Natl. Acad. Sci. USA* **2009**, *106*, 11511.
[30] P. D. Garcia, R. Sapienza, C. Lopez, *Adv. Mater.* **2010**, *22*, 12.